JOURNAL OF ENGINEERING SCIENCES

Volume 8, Issue 1 (2021)

Javanbakht T., Laurent S., Stanicki D., Salzmann I. (2021). Rheological properties of superparamagnetic iron oxide nanoparticles. Journal of Engineering Sciences, Vol. 8(1), pp. C29–C37, doi: 10.21272/jes.2021.8(1).c4

Rheological Properties of Superparamagnetic Iron Oxide Nanoparticles

Javanbakht T.[1*], Laurent S.[2, 3], Stanicki D.[2], Salzmann I.[1]

[1] Department of Chemistry and Biochemistry, Department of Physics, Concordia University, Richard J. Renaud Science Complex, 7141, Sherbrooke St., Montreal, Quebec, Canada;
[2] Laboratory of NMR and Molecular Imaging, University of Mons, Avenue Maistriau, 19, B-7000 Mons, Belgium;
[3] Center for Microscopy and Molecular Imaging (CMMI), 6041, Gosselies St., Belgium

Article info:
Received: March 25, 2021
The final version received: June 18, 2021
Accepted for publication: June 23, 2021

***Corresponding email:**
taraneh.javanbakht@concordia.ca

Abstract. The present study focuses on the rheological properties of polyethylene glycol (PEG) modified, positively charged, and negatively charged superparamagnetic iron oxide nanoparticles (SPIONs) at different temperatures. We hypothesized that the surface properties of these nanoparticles in the water did not affect their rheological properties. These nanoparticles had not the same surface properties as SPIONs-PEG had not to charge on their surface whereas positively charged and negatively charged ones with amine and carboxyl groups as their surfaces had positive and negative surface charges, respectively. However, their rheological behaviors were not different from each other. The comparative rheological study of SPIONs revealed their pseudo-Newtonian behavior. The viscosity of SPIONs decreased with the increase in temperature. At low shear rates, the shear stress of SPIONs was independent of rate and increased with the increase of rate. Moreover, at high shear rates, the shear stress for PEG-SPIONs was more than those for positively charged and negatively charged SPIONs. These measurements also revealed that at high shear rates, the shear stress of samples decreased with the increase of temperature. The shear stress of samples decreased with the increase of shear strain and the temperature. We also observed that all the samples had the same amount of shear strain at each shear stress, which indicated the exact resistance of SPIONs to deformation. Furthermore, the shear modulus decreased with time for these nanoparticles. These results suggest that these nanoparticles are promising candidates with appropriate properties for fluid processing applications and drug vectors in biomedical applications.

Keywords: rheology, SPIONs, nanomaterials, surface charge, mechanical engineering.

1 Introduction

Superparamagnetic iron oxide nanoparticles (SPIONs) have been developed for diverse applications such as magnetic drug targeting, magnetic hyperthermia, MRI contrast agent, and photocatalytic applications. These nanoparticles are usually suspended in water. They have been studied for biomedical applications [1–5], whereas a seed-meditated growth method in a nonhydrolytic condition is needed to prepare semiconductor nanocomposites for photocatalytic applications [6].

The physicochemical and biological properties of SPIONs as separated materials or in nanocomposites have been widely studied [7–11]. SPIONs exhibit the phenomenon of superparamagnetism, which corresponds to their magnetization up to their saturation magnetization when an external magnetic field is applied. They no longer exhibit any residual magnetic interaction when the magnetic field is removed. This property is size-dependent and generally manifests for nanoparticles with sizes smaller than 10 to 20 nm [5]. SPIONs can be targeted to the required area through external magnets and show interesting physical properties such as superparamagnetism, high field irreversibility, high saturation field, extra anisotropy contributions, or shifted loops after field cooling [12].

Two structural configurations are known for SPIONs : 1. a magnetic particle core usually made of magnetite, Fe_3O_4, or maghemite, γ-Fe_2O_3 coated with a biocompatible polymer, 2. nanoparticles precipitated inside a pore biocompatible polymer [13]. A polymer such as polyethylene glycol (PEG) is the best candidate for coating of SPIONs as it can reduce the natural reactivity of these nanoparticles and maintain their physical properties [14]. The coating acts to shield the magnetic particle from the surrounding environment and can also be

functionalized by attaching carboxyl and amine groups [15].

For an appropriate photocatalytic performance, iron oxides should possess a narrow bandgap value. Several techniques improve the photocatalytic performance of iron oxide semiconductor systems, such as composite heterostructure with narrow/wide bandgap, p-n heterojunctions, noble metal loading, plasmonic structure [16–18], magnetite nanoparticles can be either n-type or p-type semiconductors. However, they have the lowest resistivity among iron oxides because their bandgap is small [19].

Rheological properties of the composites of SPIONs with polymers were studied previously [11, 20–23]. However, the rheological behavior of these nanoparticles alone is needed to be investigated. Solubility is an essential characteristic of these nanoparticles for their rheological analysis. The recent synthesis of SPIONs showed that they have high solubility in water [11]. The stability of these nanoparticles depends on various factors such as their concentration, size, size polydispersity, colloidal stabilization efficiency, temperature, and magnetic field intensity [24].

This report describes the rheological behavior of three types of SPIONs at different temperatures. This work aims to investigate the rheological behavior of SPIONs coated with PEG having no charge on their surface, positively and negatively charged SPIONs at 20 °C, 40 °C, and 60 °C. To our knowledge, this is the first time that the rheological behavior of these nanoparticles is reported.

2 Research Methodology

2.1 Chemicals

We used these chemicals for the synthesis of SPIONs: methanol HPLC (ChemLab), acetone (ACS reagent), diethylic ether (ACS reagent), dimethylformamide anhydrous, n-[3-(trimethoxysilyl)propyl] ethylenediamine (TPED), which were purchased from Sigma-Aldrich. Diethylene glycol (DEG) and ferrous chloride tetrahydrate were purchased from Merck. Ferric chloride was purchased from Riedel-de Haën. 1-ethyl-3-(3-dimethyl aminopropyl) carbodiimide (EDC) and tetramethylammonium hydroxide were purchased from TCI Chemicals. 3-(triethoxysilyl)propyl succinic anhydride (TEPSA) was purchased from ABCR as described previously [10].

2.2 Synthesis of iron oxide cores

Synthesis of iron oxide cores was performed as described in our previous work [10]. Briefly, magnetite nanoparticles (NPs) were prepared by co-precipitation of iron salts in DEG [19] with mixing 8.9 g of ferrous chloride tetrahydrate salt and 9.1 ml ferric chloride in DEG (250 ml) and heating at 170 °C under a nitrogen atmosphere. After 15 min at that temperature, sodium hydroxide (15 g) was added, and the solution was stirred for 1 h at 170 °C. After cooling the mixture, the magnetic particles were isolated from the solution by magnetic decantation, and the black precipitate was washed with an aqueous solution of nitric acid (200 ml, 1 M). The dispersion of magnetite in deionized water was performed, and the dispersion was sonicated for 45 minutes and centrifuged (16.5 g; 45 min) to remove aggregates [10].

2.3 Preparation of nanoparticles

PEG-modified nanoparticles, TPED-modified nanoparticles (positively charged SPIONs), and TEPSA-modified magnetic nanoparticles (negatively charged SPIONs) were prepared as described previously [10, 11].

For the preparation of PEG-modified nanoparticles, O-(2-aminoethyl)-O'-methyl-polyethyleneglycol (120 mmol; 90 mg) was added to EDC (200 mmol; 38 mg), and TEPSA-modified ferrofluid (150 mM in iron; 5 ml) was added to the mixture. The pH was then adjusted to 7.5. After stirring the mixture for 15h at room temperature, the suspension was purified by membrane filtration [10].

Preparation of positively charged SPIONs was done with grafting N-[3-(trimethoxysilyl)propyl] ethylene-diamine (TPED) to the nanoparticles by adding TPED to a suspension of nanoparticles in nitric acid ([Fe] = 25 mM) at 50 °C. The mixture was stirred for 2 h under boiling conditions. Then it was cooled to room temperature. In the next step, the suspension was purified by membrane filtration and centrifuged (16.5 g; 45 minutes) [11].

For the preparation of negatively charged SPIONs, the suspension of obtained NPs (20 ml; [Fe] l⁄4 250 mM) was diluted with dimethylformamide (50 ml). Then water was eliminated under reduced pressure. After adding TEPSA (25 mmol; 7.1 ml) to the nanoparticle dispersion in DMF, water was added (4.3 ml). The solution of TMAOH (1 M; 2.5 mmol; 2.5 ml) was prepared at room temperature under stirring and heated to 100 °C for 24 h. The magnetic nano-objects were collected after pouring the suspension in an acetone/diethyl ether mixture (50/50). Acetone was used for washing the sample, and the precipitate was dispersed in water. Membrane filtration (membrane cut-off: 30 kDa) was performed. The NPs were then centrifuged (16 500g; 45 minutes) [11].

The surface charge measurements of positively charged and negatively charged SPIONs were reported in our previous work [25]. PEG-modified SPIOs were prepared in the current work to neutralize the surface charge of NPs in TEPSA-modified ferrofluid [26].

2.4 Rheological measurements

The rheological properties of SPIONs were studied using an Anton Paar MCR-302 rheometer. 5 mL of each sample in millipore water were prepared. Each sample contained 12 mg of magnetite nanoparticles. The concentration of SPIONs in water was 0.01 M. This concentration of SPIONs was chosen as it was low enough to be appropriate for biomedical applications, and the same concentration coated with polyethylene glycol was studied in our previous work [11]. 4 mL of each prepared sample were used for rheology. The rotational mode was applied for samples. The torque was measured at different temperatures for all the tests [27].

2.5 Statistical analysis

The QtiPlot software was used to determine the mean values and standard deviations [7]. The data were checked to be statistically significant [28]. The errors were calculated with the QtiPlot software. The data were close to each other, and the standard deviation values were small. The error bars bigger than the expected values were

attributed to the presence of polymer in the PEG-SPIONs or that of carboxyl at the surface of the neg-SPIONs, which could affect the rheological properties of nanoparticles.

3 Results

Figure 1 shows the viscosity of SPIONs versus the shear rate at 20 °C, 40 °C, and 60 °C. The applied shear rate was between 0 and 1000 s^{-1}.

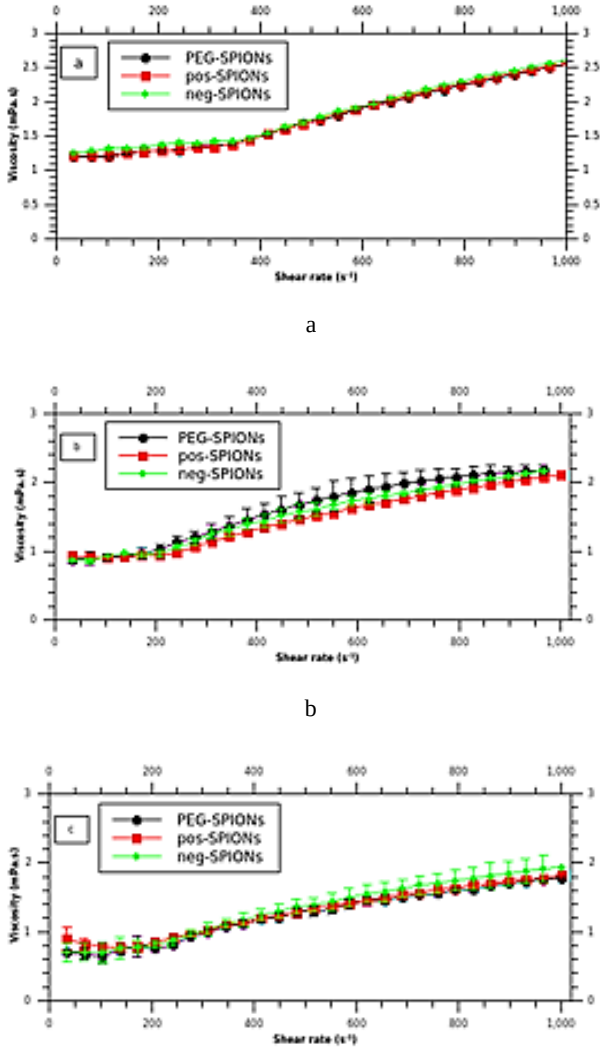

Figure 1 – Viscosity of SPIONs versus shear rate at 20 °C (a), 40 °C (b), and 60 °C (c)

As shown in Figure 1, the viscosity of SPIONs decreased with the increase of temperature by comparison of (a), (b), and (c). Moreover, their viscosity - increased between 100 and 1000 s^{-1}. Pseudo-Newtonian behavior at row shear rate is observed when shear viscosity does not change significantly, and it is invariant with the change of shear rate [29, 30].

Therefore, these nanoparticles showed a pseudo-Newtonian behavior at a shear rate less than 250 s^{-1}, increasing shear viscosity at sufficiently high shear rates.

Figure 2 shows the change of viscosity of each SPION versus shear rate at different temperatures.

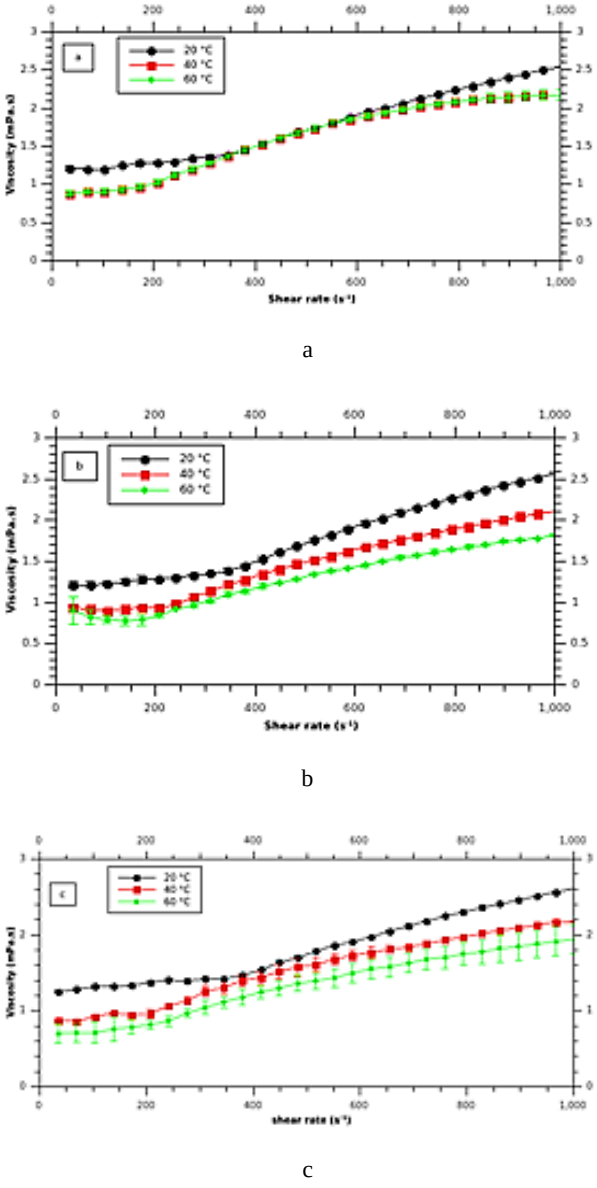

Figure 2 – Dynamic viscosity of PEG-SPIONs, positively charged SPIONs, and negatively charged SPIONs versus shear rate at 20 °C (a), 40 °C (b), and 60 °C (c)

As seen in this figure, the viscosity of SPIONs decreased with the increase of temperature. Although the same expected effect was observed for PEG-SPIONs at 40 °C and 60 °C in comparison with 20 °C, there was not a significant difference between the viscosity of these nanoparticles at 40 °C and 60 °C. This may be due to their aggregation of PEG-SPIONs at 60 °C.

The shear stress versus shear rate curves at 20 °C, 40 °C, and 60 °C are displayed in Figure 3.

As shown in Figure 3, the shear stress of increased with the increase of shear rate. At high shear rates, the shear stress for PEG-SPIONs was more than those for positively charged and negatively charged SPIONs. At high shear rates, the shear stress of samples decreased with the increase of temperature.

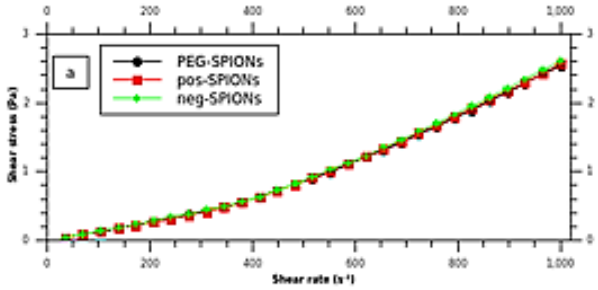

a

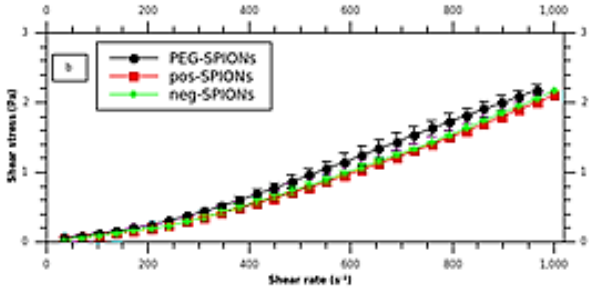

b

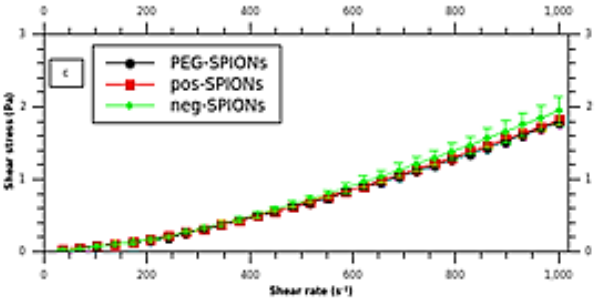

c

Figure 3 – Shear stress versus shear rate
at 20 °C (a), 40 °C (b), and 60 °C (c)

The size ratio values of positively charged and negatively charged SPIONs in nm compared to those of PEG-SPIONs measured previously with dynamic light scattering (DLS) and transmission electron microscopy (TEM) are presented in Table 1.

Table 1 – The size ratio values of positively charged and negatively charged SPIONs in nm compared to those of PEG-SPIONs

Method	Positively charged SPIONs	Negatively charged SPIONs
DLS	1.6	0.8
TEM	0.8	1.0

Comparing the results presented in Table 1, a small difference was observed in the TEM data for the size ratio values of positively and negatively charged SPIONs compared to PEG-SPIONs, whereas this difference was more for their DLS data. The larger size ratio of positively charged SPIONs was reported due to their possible aggregation [10].

Figure 4 shows torque versus time curves at 20 °C, 40 °C, and 60 °C. The torque values increased with time for SPIONs, as seen in this figure. As the concentration of samples was low, their high elasticity caused the increase of torque with time. As expected, the torque values decreased with the increase of temperature.

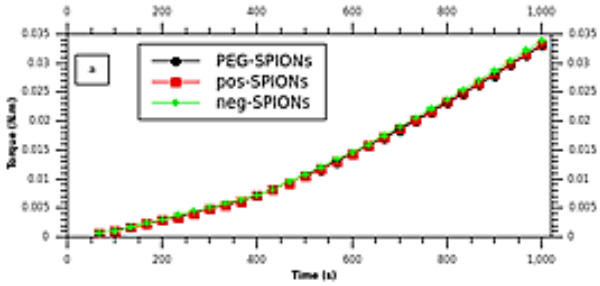

a

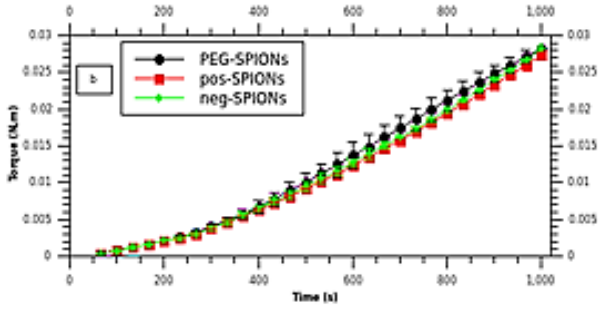

b

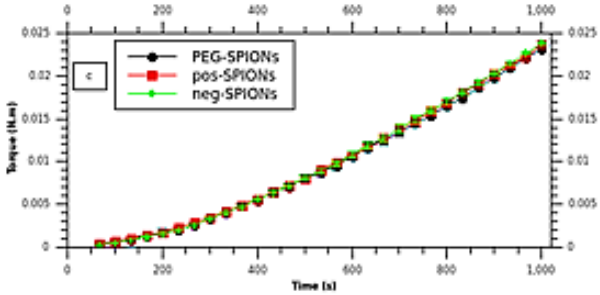

c

Figure 4 – Torque versus time
at 20 °C (a), 40 °C (b), and 60 °C (c)

The shear stress versus shear strain curves of SPIONs at 20 °C, 40 °C, and 60 °C are displayed in Figure 5.

As shown in this figure, the shear stress of samples decreased with shear strain and temperature increase. However, all the samples had the same amount of shear strain at each shear stress. This indicates that the nanoparticles were not deformed, and their resistance to the deformation was the same, although they had different surface properties that we analyzed in our previous works [10, 11].

Figure 6 shows shear stress versus shear strain curves of SPIONs at different temperatures.

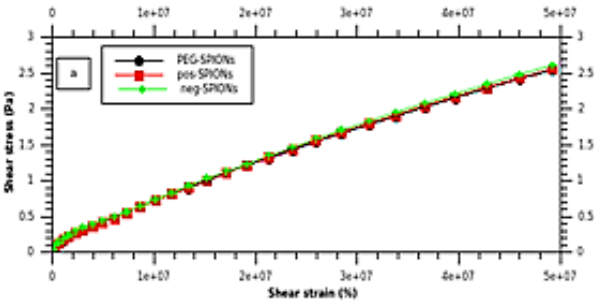

a

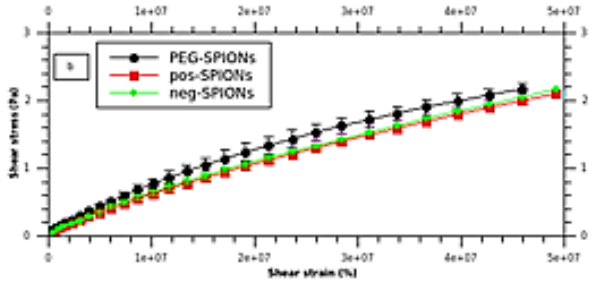

b

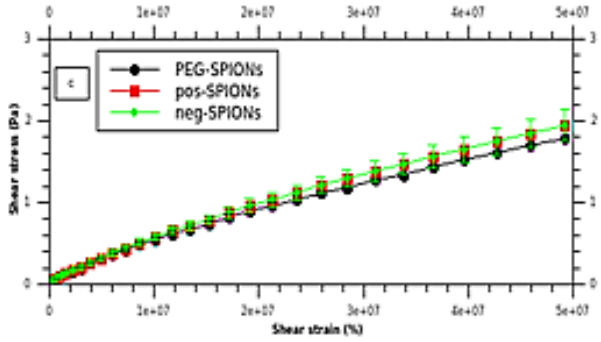

c

Figure 5 – Shear stress versus shear strain at 20 °C (a), 40 °C (b), and 60 °C (c)

As shown in Figure 6, less shear stress is required with the increase of temperature for the deformation of SPIONs. The deformation of PEG-SPIONs at 60 °C is more than that at 40 °C, whereas no change was observed for the deformation of positively and negatively charged SPIONs at these temperatures. This may be due to the surface charges of these SPIONs that hinder their deformation with the increase of temperature.

Figure 7 shows the shear modulus versus time of SPIONs at 20 °C, 40 °C, and 60 °C. As shown in this figure, shear modulus, or the ratio of shear stress to shear strain, at a low duration of time (less than 200 s), decreases with the increase of temperature. This behavior has been reported for metal-based materials previously [31]. The trend for SPIONs was not observed at low temperatures in this figure, which may be due to the difference in the surface properties of these nanoparticles. This can explain why different charged SPIONs in comparison with PEG-SPIONs have different responses to shear stress.

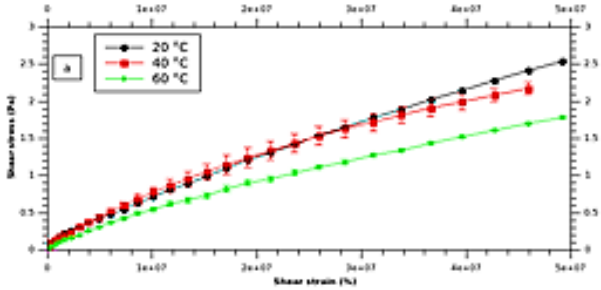

a

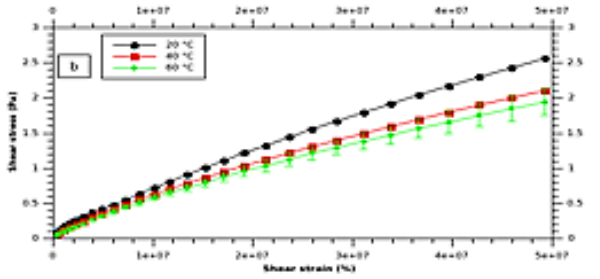

b

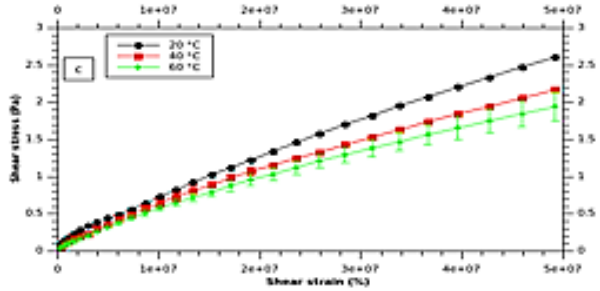

c

Figure 6 – Shear stress of PEG-SPIONs, and positively at 20 °C (a), 40 °C (b), and 60 °C (c)

4 Discussion

Shear modulus was very low for SPIONs, and its values decreased with time for all the samples. Moreover, the shear modulus was independent of time after 400 s because this modulus did not change with time after this duration.

An important parameter that reflects the material's ability to resist deformation is shear modulus, which is the ratio of shear stress to shear strain. Shear modulus decreases with time, but it becomes constant after 8 minutes for all the samples. Moreover, this parameter decreases with the increase of temperature. This means that the deformation of SPIONs can happen by applying less amount of shear stress as the temperature increases.

The decrease of viscosity with the increase of temperature has been previously reported [32]. With the increase of temperature, Brownian motion enhances, which caused the decreased interaction between the nanoparticles. Therefore, the flow resisting force and heat resistance in samples decrease. This phenomenon is helpful to improve the efficiency of SPIONs as solar absorbers at high temperatures [33].

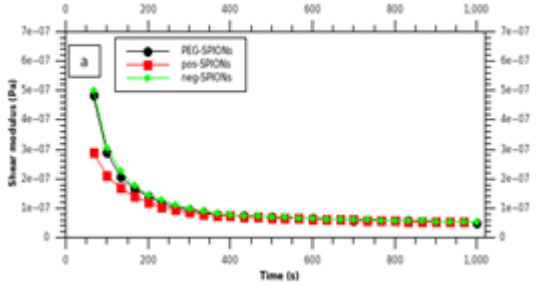

a

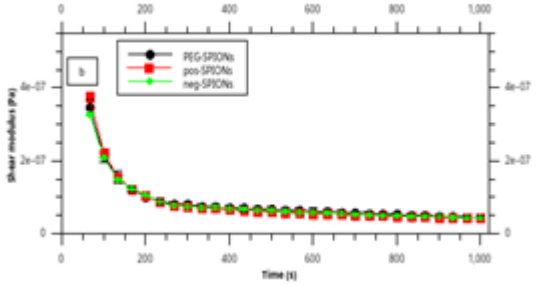

b

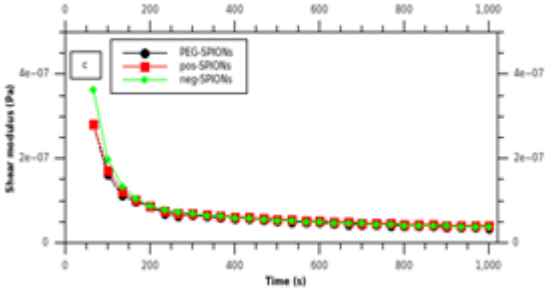

c

Figure 7 – Shear modulus versus time
at 20 °C (a), 40 °C (b), and 60 °C (c)

The rheological behavior of SPIONs depends on their physical properties. Their pseudo-Newtonian behavior can be affected by the volume, size distribution, and shape of the particles. It should be noted that this behavior can also depend on the concentration, in proportion to some maximum packing fraction partly controlled by the form of the particle size distribution [34].

According to our previous investigation with dynamic light scattering, the average sizes of PEG-SPIONs, positively charged and negatively charged SPIONs were 19.3 ± 0.1 nm, 30.6 ± 0.1 nm, and 15.7 ± 0.2 nm, respectively [10].

The independence of shear stress from the shear rate at low rates for SPIONs corresponds to their yield behavior, which is accounted for by their elastic behavior [35].

This was reported for iron oxide suspensions in silicone oil previously [36]. The identical behavior of SPIONs concerning the independence of shear stress from the shear rate at low rates indicates that they have the same rheological behavior at a constant temperature.

At high shear rates for a given shear strain, the flow stress decreases with increasing temperature. This phenomenon is more pronounced at higher strain rates and more significant strains and can be attributed to the temperature rise generated in the samples because of deformation heating [37].

The increase of torque with time, as observed in our experiments, is due to the elasticity of the samples. [38]. More investigation is required to determine the viscoelastic properties of SPIONs with oscillatory rheology.

We observed that the shear modulus for SPIONs decreased with the increase of temperature. The decrease of shear modulus with increased temperature has been reported previously for other materials [39][40]. The rheological analysis of SPIONs in oscillatory mode will be performed in further investigation.

Another important topic to consider is that the optimal surface charge of SPIONs for their diverse applications should be close to neutral or slightly negative [41].

However, the surface charge affects the zeta potential and that, in turn, the zeta potential determines the solution stability of these nanoparticles [7, 11]. We seek to improve the application of these nanoparticles as future semiconductors in solar cell fabrication as similar nanoparticles, when prepared with irradiation, could have a uniform shape appropriate for this application [42]. The next step will be to determine their electrochemical properties. As the nanostructure of materials impacts their electrical characteristics, it would be necessary to investigate the effect of the structure of these nanoparticles or other nanoparticles on their physical properties for their applications in solar cells [42–45].

Previously, some devices' physical and biological properties were studied with different methods [46–49]. The physicochemical properties of some polymers and nanomaterials have also been investigated during recent years [50–53]. The rheological properties of some biological materials [54–57] will be studied in our subsequent investigation.

The viscosity of blood at 37 °C is around 3 mPa·s. The measured viscosity of SPIONs in this study was less than that of blood [58, 59]. Therefore, these nanoparticles have been appropriate tools to be used in biomedical applications. More investigations are required to determine the rheological properties of SPIONs in oscillatory mode and those of the materials used in these devices or conjugation with these nanoparticles.

5 Conclusions

The rheological properties of SPIONs dispersed in water affect their behavior for their various applications. These properties were analyzed and designed to meet the requirements of these applications.

The obtained results indicate that the surface properties of SPIONs do not affect their rheological properties at different temperatures as three types of SPIONs with different surface properties that we reported previously showed the same rheological behavior.

Some issues are required to be addressed, and among these, the viscoelasticity of these nanoparticles is an important rheological property and of great interest as their viscosity affects the drug delivery output when these nanoparticles are used as drug vectors. It is also required to proceed with novel functionalizations of SPIONs to obtain new nanoparticles with surface modifications that can affect their rheological behavior. Progress in this issue will allow precise tuning of the properties of these nanoparticles for their fluid processing and semiconductor applications.

References

1. Rosensweig, R. W. (1985). *Ferrohydrodynamics (Cambridge Monographs on Mechanics and Applied Mathematics)*. Cambridge, Cambridge University Press.
2. Sabale, S., Kandesar, P., Jadhav, V., Komorek, R., Motkuri, R. K., Yu, W.-Y. (2017). Recent developments in the synthesis, properties, and biomedical applications of core/shell superparamagnetic iron oxide nanoparticles with gold. *Biomaterials Science*. Vol. 5(11), pp. 2212–2225. https://doi.org/10.1039/c7bm00723j.
3. Lin, M. M., Kim, D. K., Haj, A. J. E., Dobson, J. (2009). Development of superparamagnetic iron oxide nanoparticles (SPIONS) for translation to clinical applications. *IEEE Transactions on NanoBioscience*, Vol. 7(4), pp. 298–305. https://doi.org/10.1109/TNB.2008.2011864.
4. Kaushik, S., Thomas, J., Panwar, V., Ali, H., Chopra, V., Sharma, A., Tomar, R., Ghosh, D. (2020). In situ biosynthesized superparamagnetic iron oxide nanoparticles (SPIONS) induce efficient hyperthermia in cancer cells. *ACS Applied Bio Materials*, Vol. 3(2), pp. 779–788. https://doi.org/10.1021/acsabm.9b00720.
5. Wahajuddin, A. S. (2012). Superparamagnetic iron oxide nanoparticles: magnetic nanoplatforms as drug carriers. *International Journal of Nanomedicine*, Vol. 7, pp. 3445–3471. https://doi.org/10.2147/IJN.S30320.
6. Chiu, W., Khiew, P., Cloke, M., Isa, D., Lim, H., Tan, T., Huang, N., Radiman, S., Abd-Shukor, R., Hamid, M.A.A., Chia, C. (2010). Heterogeneous seeded growth: synthesis and characterization of bifunctional Fe3O4/ZnO core/shell nanocrystals. *Journal of Physical Chemistry C*, Vol. 114(18), pp. 8212–8218. https://doi.org/10.1021/jp100848m.
7. Graczyk, H., Bryan, L. C., Lewinski, N., Suarez, G., Coullerez, G., Bowen, P., Riediker, M. (2015). Physicochemical Characterization of NebulizedSuperparamagnetic Iron Oxide Nanoparticles (SPIONs). *Journal of Aerosol Medicine and Pulmonary Drug Delivery*, Vol. 28(1), pp. 43–51. https://doi.org/10.1089/jamp.2013.1117.
8. Mieloch, A. A., Zurawek, M., Giersig, M., Roswadowska, N., Rybka, J. D. (2020). Bioevaluation of superparamagnetic iron oxide nanoparticles (SPIONs) functionalized with dihexadecyl phosphate (DHP). *Scientific Reports*, Vol. 10(1), 2725. https://doi.org/10.1038/s41598-020-59478-2.
9. Belanova, A. A., Gavalas, N., Makarenko, Y. M., Belousova, M. M., Soldatov, A. V., Zolotukhin, P. V. (2018). Physicochemical properties of magnetic nanoparticles: implications for biomedical applications in vitro and in vivo. *Oncology Research and Treatment*, Vol. 41(3), pp. 139–143. https://doi.org/10.1159/000485020.
10. Javanbakht, T., Laurent, S., Stanicki, D., Frenette, M. (2020). Correlation between physicochemical properties of superparamagnetic iron oxide nanoparticles and their reactivity with hydrogen peroxide. *Canadian Journal of Chemistry*, Vol. 98(10), pp. 601–608. https://doi.org/10.1139/cjc-2020-0087.
11. Javanbakht, T., Laurent, S., Stanicki, D., David, E. (2019). Related physicochemical, rheological, and dielectric properties of nanocomposites of superparamagnetic iron oxide nanoparticles with polyethyleneglycol. *Journal of Applied Polymer Science*, Vol. 137(3), pp. 48280–48289. https://doi.org/10.1002/app.48280.
12. Grancharov, S. G., Zeng, H., Sun, S. H., Wang, S. X., O'Brien, S., Murray, C. B., Kirtley, J. R. G., Held, A. (2005). Bio-functionalization of monodisperse magnetic nanoparticles and their use as biomolecular labels in a magnetic tunnel junction based sensor. *Journal of Physical Chemistry B*, Vol. 109(26), pp. 13030–13035. https://doi.org/10.1021/jp051098c.
13. Hans, M. L., Lowman, A. M. (2002). Biodegradable Nanoparticles for Drug Delivery and Targeting. *Current Opinion in Solid State and Materials Science*, Vol. 6(4), pp. 319–327. https://doi.org/10.1016/S1359-0286(02)00117-1.
14. Solar, P., González, G., Vilos, C., Herrera, N., Juica, N., Moreno, M., Simon, F., Velásquez, L. (2015). Multifunctional polymeric nanoparticles doubly loaded with SPION and ceftiofur retain their physical and biological properties. *Journal of Nanobiotechnology*, Vol. 13(14), pp. 14–25. https://doi.org/10.1186/s12951-015-0077-5.
15. Andrade, A., Ferreira, R., Fabris, J., Domingues, R. (2011). Coating Nanomagnetic Particles for Biomedical Applications. *Biomedical engineering - Frontiers and Challenges*, North Dakota, University of North Dakota.
16. Qu, Y., Duan, X. (2013). Progress, challenge and perspective of heterogeneous photocatalysts. *Chemical Society Reviews*, Vol. 42(7), pp. 2568–2580. https://doi.org/10.1039/C2CS35355E.
17. Xu, P., Zeng, G. M., Huang, D. L., Feng, C. L., Hu, S., Zhao, M. H., Lai, C., Wei, Z., Huang, C., Xie, G. X., Liu, Z. F. (2012). Use of iron oxide nanomaterials in wastewater treatment: a review. *Science of the Total Environment*, Vol. 424, pp. 1–10. https://doi.org/10.1016/j.scitotenv.2012.02.023.
18. Wang, Y., Wang, Q., Zhan, X., Wang, F., Safdar, M., He, J. (2013). Visible light driven type II heterostructures and their enhances photocatalysis properties: a review. *Nanoscale*, Vol. 5(18), pp. 8326–8339. https://doi.org/10.1039/c3nr01577g.
19. Boxall, C., Kelsall, G. Zhang, Z. (1996). Photoelectrophoresis of colloidal iron oxides. Part 2. – Magnetite (Fe_3O_4). *Journal of the Chemical Society, Faraday Transactions*. Vol. 92(5), pp. 791–802. https://doi.org/10.1039/FT9969200791.

20. Brullot, W., Reddy, N. K., Wouters, J., Valev, V. K., Goderis, B., Vermant, J., Verbiest, T. (2012). Versatile ferrofluids based on polyethylene glycol coated iron oxide nanoparticles. *Journal of Magnetism and Magnetic Materials*, Vol. 324(11), pp. 1919–1925. https://doi.org/10.1016/j.jmmm.2012.01.032.
21. Gonçalves, L. C., Seabra, A. B., Pelegrino, M. T., de Araujo, D. R., Bernardes, J. S., Haddad, P. S. (2017). Superparamagnetic iron oxide nanoparticles dispersed in Pluronic F127 hydrogel: potential uses in topical applications. *RSC Advances*, Vol. 7(24), pp. 14496–14503. https://doi.org/10.1039/C6RA28633J.
22. Nejatpour, M., Unal, U., Acar, H. Y. (2020). Bidisperse magneto-rheological fluids consisting of functional SPIONs added to commercial MRF. *Journal of Industrial and Engineering Chemistry*, Vol. 91, pp. 25, 110–120. https://doi.org/10.1016/j.jiec.2020.07.040.
23. Yoon, K. Y. (2012). *The Design and Control of Stability and Magnetic Properties of Imaging Nanoparticles*. PhD thesis, University of Texas, Austin.
24. Socoliuc, V., Bica, D., Vekas, L. (2011). Magnetically induced phase condensation with asymptotic critical temperature in an aqueous magnetic colloid. *Magnetohydrodynamics*, Vol. 47(2), pp. 201–206. https://doi.org/10.22364/mhd.47.2.12.
25. Stanicki, D., Boutry, S., Laurent, S., Wacheul, L., Nicolas, E.. Crombez, D., Elst, L. V., Lafontaine, D. L. J., Muller, R. N. (2014). Carboxy-silane coated iron oxide nanoparticles: A convenient platform for cellular and small animal imaging. *Journal of Materials Chemistry B*, Vol. 2(4), pp. 387–397. https://doi.org/10.1039/C3TB21480J.
26. Cu, Y., Saltzman, W. M. (2009). Controlled Surface Modification With Poly(ethylene)glycol Enhances Diffusion of PLGA Nanoparticles in Human Cervical Mucus. *Molecular Pharmacology*, Vol. 6(1), pp. 173–181. https://doi.org/10.1021/mp8001254.
27. Fathurrohman, M. I., Maspanger, D. R., Sutrisno, S. (2015). Vulcanization Kinetics and Mechanical Properties of Ethylene Propylene Diene Monomer Thermal Insulation. *Bulletin of Chemical Reaction Engineering and Catalysis*, Vol. 10(2), pp. 104–110. https://doi.org/10.9767/bcrec.10.2.6682.104-110.
28. Javanbakht, T., Ghane-Motlah, B., Sawan, M. (2020). Comparative study of antibiofilm activity and physicochemical properties of microelectrode arrays. *Microelectronic Engineering*, Vol. 229, 111305. https://doi.org/10.1016/j.mee.2020.111305.
29. Haward, S. J., McKinley, J. H. (2012). Stagnation point flow of wormlike micellar solutions in a microfluidic cross-slot device: Effects of surfactant concentration and ionic environment. *Physical Review E*, Vol. 85(3), 031502. https://doi.org/10.1103/PhysRevE.85.031502.
30. Jamali, S., Armstrong, R. C., Mc Kinley, G. H. (2019). Multiscale nature of thixotropy and rheological hysteresis in attractive colloidal suspensions under shear. *Physical Review Letters*, Vol. 123(24), 248003. https://doi.org/10.1103/PhysRevLett.123.248003.
31. Liu, Z. Y., Wang, G., Chan, K. C., Ren, J. L., Huang, Y. J. Bian, X. L., xu, X. H., Zhang, D. S., Gao, Y. L., Zhai, Q. J. (2013). Temperature dependent dynamics transition of intermittent plastic flow in a metallic glass. I. Experimental investigations. *Journal of Applied Physics*, Vol. 114, 033520. https://doi.org/10.1063/1.4815943.
32. Chen, H. J., Wang, Y. M., Qu, J. M., Hong, R. Y., Li, H. Z. (2011). Preparation and characterization of silicon oil based ferrofluid. *Applied Surface Science*, Vol. 257(24), pp. 10802–10807. https://doi.org/10.1016/j.apsusc.2011.07.103.
33. Han, D., Meng,, Z., Wu, D., Zhang, C., Zhu, H. (2011). Thermal properties of carbon black aqueous nanofluids for solar absorption. *Nanoscale Research Letters*, Vol. 6(1), pp. 457. https://doi.org/doi:10.1186/1556-276X-6-457.
34. Barnes, H.A. (1989). Shear-Thickening ("Dilatancy") in Suspensions of Nonaggregating Solid Particles Dispersed in Newtonian Liquids. *Journal of Rheology*, Vol. 33(2), pp. 329–366. https://doi.org/10.1122/1.550017.
35. Vu-Bac, N., Areias, P., Rabczuk, T. (2016). A multiscale multisurface constitutive model for the thermo-plastic behavior of polyethylene. *Polymer*, Vol. 105, pp. 327–338. https://doi.org/10.1016/j.polymer.2016.10.039.
36. Yang, M. C., Scriven, L. E., Makosco, C. W. (1986). Some rheological measurements on magnetic iron oxide suspensions in silicone oil. *Journal of Rheology*, Vol. 30(5), pp. 1015–1029. https://doi.org/10.1122/1.549892.
37. Chen, T. -H., Tsai, C. -K., Fang, T. -H. (2013). Dynamic shear characteristic and fracture fature of inconel 690 alloy under different high strain rates and temperatures. *Advances in Material Science and Engineering*, Vol. 2013, 382503. https://doi.org/10.1155/2013/382503.
38. Sumith, S., Sangam, K., Kannan, K., Shankar, K. (2020). Prediction of nonlinear viscoelastic behaviour of simulative soil for deep-sea sediment using a thermodynamically compatible model. *Inverse Problems in Science and Engineering*, Vol. 28(6), pp. 1741–5977. https://doi.org/10.1080/17415977.2019.1648452.
39. Todd, T. P. (1973). Effect of cracks on elastic properties of low porosity rocks. PhD thesis, University of Toronto.
40. Hua, X., Wang, L., Yang, S. (2019). Molecular dynamics simulation of improving the physical properties of polytetrafluoroethylene cable insulation materials by boron nitride nanoparticle under moisture-temperature-electric fields conditions. *Polymers*, Vol. 11(6), pp. 971–985. https://doi.org/10.3390/polym11060971.
41. Durymanov, M. O., Rosenkranz, A. A, Sobolev, A. S. (2015). Current approaches for improving intratumoral accumulation and distribution of nanomedicines. *Theranostics*, Vol. 5(9), pp. 1007–1020. https://doi.org/10.7150/thno.11742.
42. Hussain, D. H., Abdulah, H. I., Rheima, A. M. (2016). Synthesis and characterization of ɣ-Fe2O3 nanoparticles photoanodeby novel method for dye sensitized solar cell. *International Journal of Scientific Research and Publications*, Vol. 6(10), pp. 26–31.
43. Cai, F., Zhang, S., Yuan, Z. (2015). Effect of magnetic gamma-iron oxide nanoparticles on the efficiency of dye-sensitized solar cells. RSC Advances, Vol. 5(53), pp. 42869–42874. https://doi.org/10.1039/C5RA05936D.
44. Tuharin, K., Turek, Z., Zanáška, M., Kudrna, P., Tichý, M. (2020). Iron oxide and iron sulfide films prepared for dye-sensitized solar cells. *Materials*, Vol. 13(8), 1797. https://doi.org/doi:10.3390/ma13081797.

45. Tharwat, M. M., Almalki, A., Mahros, A. M. (2021). Plasmon-enhanced sunlight harvesting in thin-film solar cell by randomly distributed nanoparticle array. *Materials*, Vol. 14(6), 1380. https://doi.org/10.3390/ma14061380.
46. Ghane-Motlagh, B., Javanbakht, T., Shoghi, F., Wilkinson, K. J., Martel, R., Sawan, M. (2016). Physicochemical properties of peptide-coated microelectrode arrays and their in vitro effects on neuroblast cells. *Materials Science and Engineering C*, Vol. 68, pp. 642–650. https://doi.org/10.1016/j.msec.2016.06.045.
47. Djavanbakht, T., Carrier, V., André, J. -M., Barchewitz, R., Troussel, P. (2000). Effets d'un chauffage thermique sur les performances de miroirs multicouches Mo/Si, Mo/C et Ni/C pour le rayonnement X mou. *Journal de Physique IV France*, Vol. 10, pp. 281–287. https://doi.org/10.1051/jp4:20001031.
48. Tsutsumi, Y., Niinomi, M., Nakai, M., Shimabukuro, M., Ashida, M., Chen, P., Doi, H., Hanawa, T. (2016). Electrochemical surface treatment of a β-titanium alloy to realize an antibacterial property and bioactivity. *Metals*, Vol. 6(4), 76. https://doi.org/10.3390/met6040076.
49. Kiran, A. S. K., Sireesha, M., Ramalingam, R., Kizhakeyil, A., Verma, N. K., Lakshminarayanan, R., Kumar, T. S. S., Doble, M., Ramakrishna, S. (2019). Modulation of biological properties by grain refinement and surface modification on titanium surfaces for implant-related infections. *Journal of Materials Science*, Vol. 54(20), pp. 13265–13282. https://doi.org/10.1007/s10853-019-03811-2.
50. Javanbakht, T., Bérard, A., Tavares, J. R. (2016). Polyethylene glycol and poly (vinyl alcohol) hydrogels treated with photo-initiated chemical vapor deposition. *Canadian Journal of Chemistry*, Vol. 94(9), pp. 744–750. https://doi.org/10.1139/cjc-2016-0229.
51. Javanbakht, T., David, E. (2020). Rheological and physical properties of a nanocomposite of graphene oxide nanoribbons with polyvinyl alcohol. *Journal of Thermoplastic Composite Matererials*, 0892705720912767. https://doi.org/10.1177/0892705720912767.
52. Javanbakht, T., Hadian, H., Wilkinson, K. J. (2020). Comparative study of physicochemical properties and antibiofilm activity of graphene oxide nanoribbons. Journal of Engineering Sciences, Vol. 7(1), pp. C1–C8. https://doi.org/10.21272/jes.2020.7(1).c1.
53. Javanbakht, T., Sokolowski, W. (2015). *Thiolene/Acrylate Systems for Biomedical Shape-Memory Polymers in Shape Memory Polymers for Biomedical Applications (Ed. L'H Yahia)*, pp. 157–166, Sawston, Cambridge, Woodhead Publishing.
54. Sicilia, G., Grainger-Boultby, C., Francini, N., Magnusson, J. P., Saeed, A. O., Fernández-Trillo, F., Spain, S. G., Alexander, C. (2014). Programmable polymer-DNA hydrogels with dual input and multiscale responses. *Biomaterial Sciences*, Vol. 2, pp. 203–211. https://doi.org/10.1039/C3BM60126A.
55. Bravo-Anaya, L. M., Pignon, F., Martínez, F. A. S., Rinaudo, M. (2016). Rheological properties of DNA molecules in solution: molecular weight and entanglement influences. *Polymers*, Vol. 8(8), 279. https://doi.org/10.3390/polym8080279.
56. Djavanbakht, T., Jolès, B., Laigle, A. (2000). Intracellular stability of antisense oligonucleotides protected by the d(GCGAAGC). *Biomedical Society Transactions*, Vol. 28, p. A201. https://doi.org/10.1042/bst028a201c.
57. Murray, B. S. (2011). Rheological properties of protein films. *Current Opinion in Colloid and Interface Science*, Vol. 16(1), pp. 27–35. https://doi.org/10.1016/j.cocis.2010.06.005.
58. Farina, A., Fasano, A., Rossi, F. (2021). Mathematical models for some aspects of blood microcirculation. *Symmetry*, Vol. 13, 1020. https://doi.org/10.3390/sym13061020.
59. Hijikata, W., Rao, J., Abe, S., Takatani, S., Shinshi, T. (2015). Estimating flow rate using the motor torque in a rotary blood pump. *Sensors and Materials*, Vol. 27(4), pp. 297–308. https://doi.org/10.18494/SAM.2015.1128.